SCIENTIFIC REP⚙RTS

OPEN

An Interfacial Europium Complex on SiO$_2$ Nanoparticles: Reduction-Induced Blue Emission System

Ayumi Ishii & Miki Hasegawa

In this study, Eu-coated SiO$_2$ nanoparticles have been prepared, consisting of an interfacial complex of Eu and 1,10-phenanthroline (phen) at the solid surfaces of the SiO$_2$/Eu nanostructures. The as-prepared SiO$_2$/Eu/phen nanoparticles exhibits sharp red emission via energy transfer from the phen to the Eu^{III}. After sintering at 200 °C in air, the emission is tuned from red to blue. The blue emission is originated from Eu^{II}. This reduction-induced emissive phenomenon resulted from the electron-donating environment created by the surrounding phen and SiO$_2$, which is the first reported fabrication of a stable Eu^{II}-based emissive material using mild conditions (reaction in air and at low temperature) and an organic-inorganic hybrid nanostructure. The existence of two different stable oxidation states with characteristic emissions, blue emissive Eu^{II} and red emissive Eu^{III}, suggests significant potential applications as novel luminescent materials with inorganic-organic hybrid structures.

Interfacial nanostructures formed by organic and inorganic materials have great potential to exhibit novel properties not displayed by the original components. The suitable design of such interfaces is the key to fabricating functional organic-inorganic hybrid materials for applications in photonics[1–4], electronics[5–7], magnetic devices[8,9] and catalyses[10,11]. Our current research is focused on constructing functional interfaces through the complexation of organic and inorganic materials, with the aim of stabilizing and tuning the photo-physical properties associated with luminescent materials, such as lanthanide compounds.

Here we demonstrate the development of a novel reduction-induced emission system by forming interfacial europium (Eu) complexes on SiO$_2$ nanoparticles. The variations in the luminescence properties of Eu ions with changes in their valence state have been widely investigated in many host materials, and it is known that divalent and trivalent Eu ions luminesce in the blue and red spectral regions, respectively. The divalent Eu ion (Eu^{II}) shows a broad emission band assigned to the allowed 4f^{6}5d → 4f^7 electric dipole transition, a phenomenon that has been reported in inorganic host materials such as sulfates, phosphates, borates, silicates and aluminates[12]. The trivalent Eu ion (Eu^{III}) shows some narrow emission bands assigned to the electric dipole forbidden (Laporte forbidden) transition of the inner-shell 4f orbitals. The existence of two different oxidation states with characteristic emissions as well as the high emission efficiency of Eu^{II} and the high colour purity of Eu^{III} is predicted to allow the fabrication of novel luminescent materials for a wide range of applications, in the event that a process is found that allows the desired species to be readily selected.

There are no natural sources containing Eu^{II}. The emission of Eu^{II} is of significantly higher intensity than that of Eu^{III} in any inorganic host material. Thus, in order to prepare luminescent materials containing Eu^{II}, it is necessary to reduce Eu^{III} to Eu^{II} in an appropriate matrix, using a reducing atmosphere at temperatures above 1000 °C[13–18]. Although some reports show that this reduction occurs even in air, high temperatures are still necessary, along with a rigid inorganic crystal structure as a host[19–21]. In contrast, Eu^{III} emission can be easily and efficiently obtained by complexation with organic compounds. In such cases, an organic compound having a high absorption coefficient transfers its photo-excitation energy to

College of Science and Engineering, Aoyama Gakuin University, 5-10-1 Fuchinobe, Chuo-ku, Sagamihara, Kanagawa, 252-5258, Japan. Correspondence and requests for materials should be addressed to A.I. (email: ayumi@chem.aoyama.ac.jp) or M.H. (email: hasemiki@chem.aoyama.ac.jp)
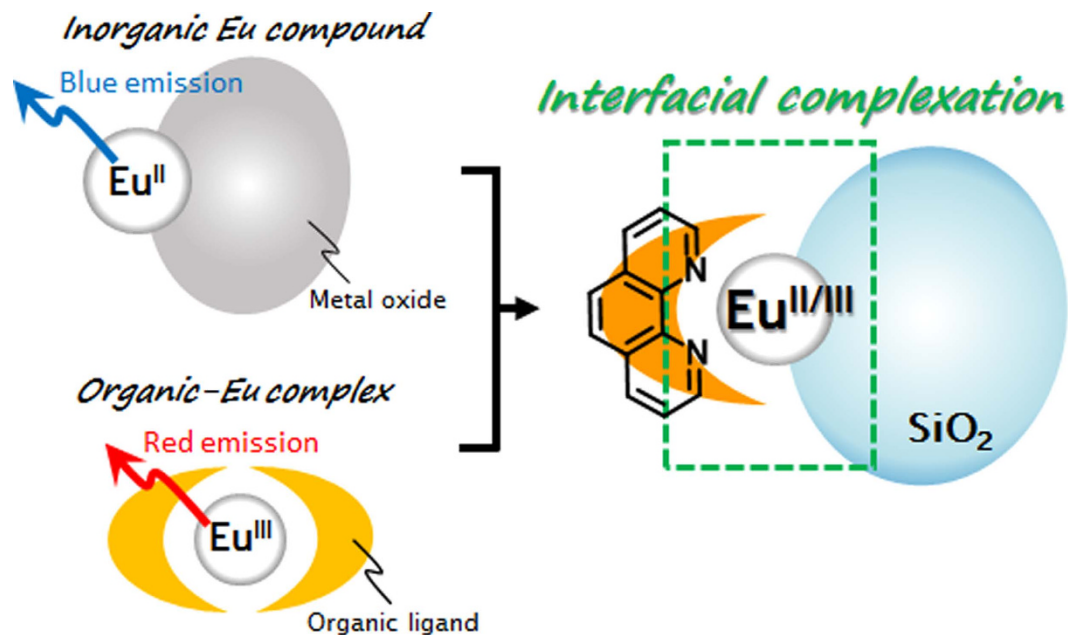
Figure 1. Schematic illustration of SiO₂ nanoparticles coated with Eu ions followed by complexation with phen at the interface.

the Eu ions. The organic compound in the complex not only plays an important role as an energy donor for the Eu ions, but is also able to control the structures and arrangements of the emissive substances at a molecular level through coordination bonds. It is thus expected that a combination of an inorganic matrix with organic compounds will produce novel luminescent materials in which the performance of the Eu ion is enhanced.

In the present study, we have prepared SiO_2 nanoparticles coated with Eu ions and discovered that an interfacial complex of Eu and 1,10-phenanthroline (phen) forms at the solid surfaces of the SiO_2/Eu nanostructures, as illustrated in Fig. 1. SiO_2 nanoparticles were chosen as host materials because of their high availability and thermal stability. This hybrid nanostructure at the interface between inorganic and organic compounds induced significant visible light emission from two different stable oxidation states of the Eu ions.

Results And Discussion

To coat the SiO_2 surfaces with Eu ions, SiO_2 nanoparticles (20~50 nm) were immersed in a 50 mM ethanol solution of $EuCl_3$ at 70 °C for 30 min, resulting in coating of Eu ions on the SiO_2 surfaces (this material hereafter referred to as SiO_2/Eu). This colloidal suspension containing the SiO_2 and Eu ion was subsequently dropped onto a quartz substrate that was then dried at 110 °C for 15 min. In previous reports, interfacial complexation with anthraquinone or cyclopentadiene has been demonstrated at the solid surface of TiO_2, and has been shown to function as an excellent visible light absorber for photo-electric conversion[22,23]. Accordingly, the SiO_2/Eu nanoparticles were immersed in an ethanol solution of phen at 75 °C for 60 min to form a new material (SiO_2/Eu/phen). The phen molecule is known to coordinate to Eu ions in a bidentate fashion through bonding of two nitrogen atoms[24,25]. In the present work, phen was also assumed to form an interfacial complex with Eu ions at the solid surfaces of the SiO_2/Eu nanostructures. X-ray photoelectron spectroscopy (XPS) measurements demonstrated the formation of coordination bonds between phen molecules and Eu ions on the SiO_2/Eu nanoparticles. In the resulting data, the N1s XPS band of phen at 396.7 eV was shifted to 399.7 eV on the higher energy side, indicating that the phen coordinated to the Eu ions on the SiO_2 nanoparticles (Fig. S1)[26]. The phen molecule never coordinates the surface of SiO_2 nanoparticles without Eu ions. It suggests that Eu ions exist on the surface of SiO_2 nanoparticle and form the complexes at the interface between SiO_2 nanoparticles and phen ligands.

Fig. 2 shows scanning electron microscope (SEM) images of SiO_2 nanoparticles coated with Eu ions. Compared with SiO_2 nanoparticles (Fig. S2), the SiO_2/Eu particles exhibit close packing between themselves. The average SiO_2 particle size of 20 nm was almost unchanged by the addition of the Eu ions to the surface, indicating that the ions formed a nano-ordered thin film layer. Energy dispersive X-ray spectroscopy (EDS) was used to determine the elemental compositions, as shown in Fig. 2c. The EDS spectrum confirmed the presence of Si, O, and Eu. Since no Cl peaks were evident around 2.6 keV, we may conclude that Eu oxides or hydroxides were formed on the SiO_2 nanoparticles through the colloidal suspension process.
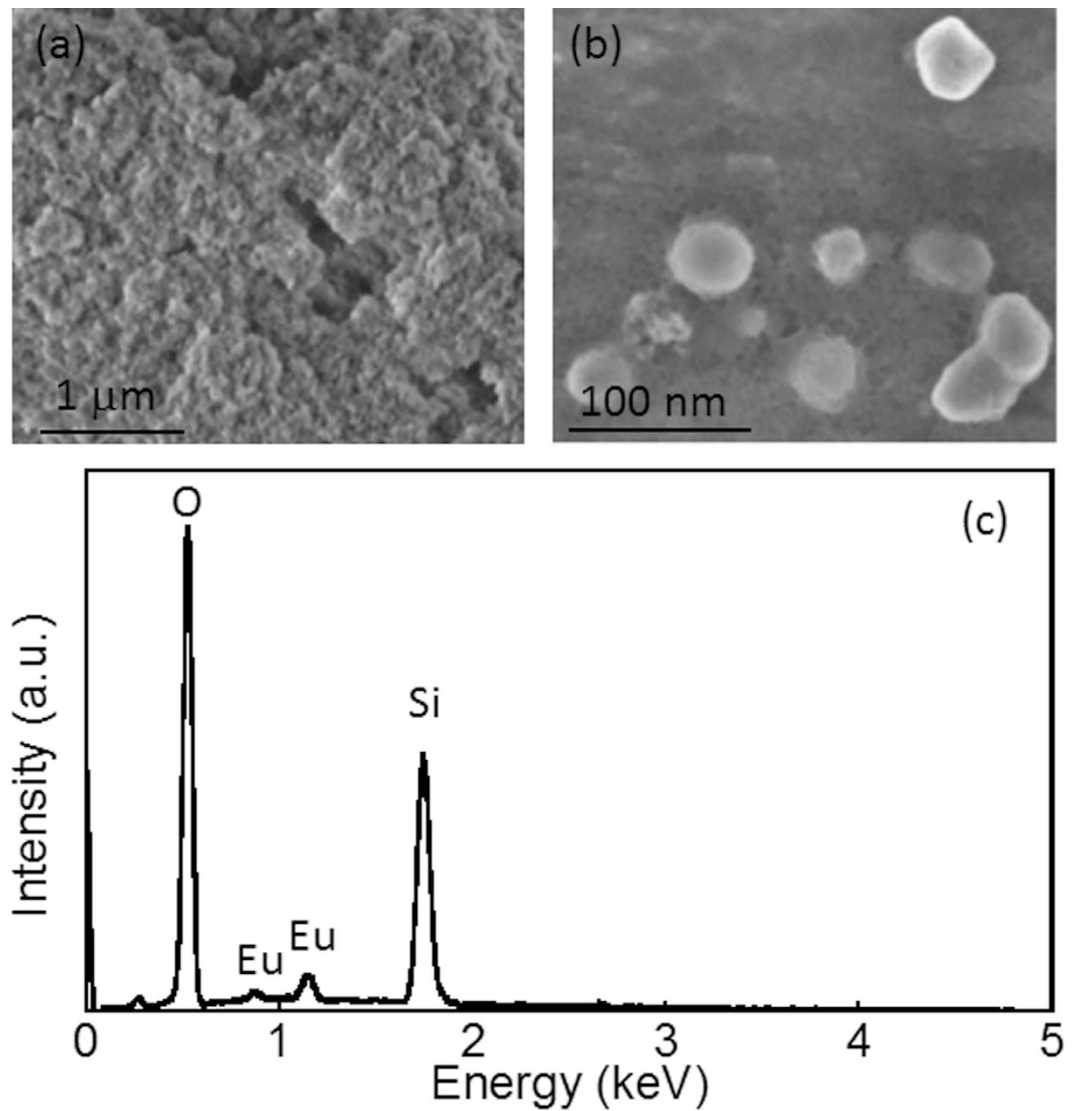
Figure 2. a) Low and **b**) high magnification SEM images of SiO_2/Eu nanoparticles and **c**) the EDS pattern obtained from SiO_2/Eu nanoparticles.
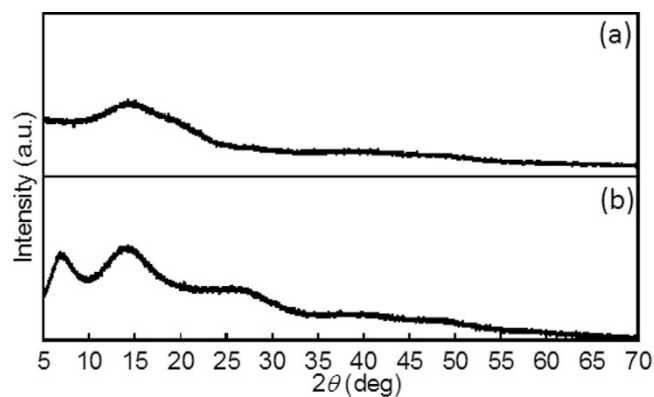

Figure 3. Synchrotron XRPD patterns obtained from a) SiO_2 and **b**) SiO_2/Eu nanoparticles ($\lambda = 0.99933$ Å).

Based on the synchrotron X-ray powder diffraction (XRPD) patterns in Fig. 3a, the SiO_2 nanoparticles had an amorphous structure with a broad peak at approximately 15°[27], with an additional diffraction peak at 7.1° observed in the SiO_2/Eu pattern (Fig. 3b). The additional peak indicates the formation of Eu
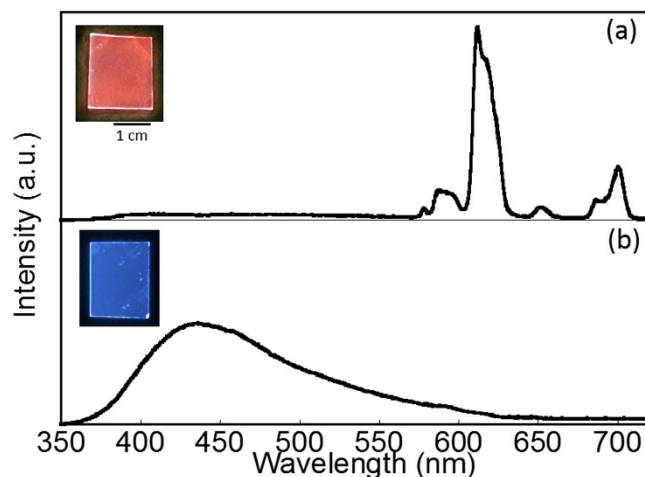
Figure 4. Luminescence spectra of a) as-prepared and **b)** sintered SiO$_2$/Eu/phen nanoparticles ($\lambda_{ex} = 280$ nm). Insets show photographic images of each sample on glass substrates under UV irradiation. 385 nm band of a) is due to a tail of the ligand-centered emission of phen moiety filtered by a UV cut filter.

crystal shells around the SiO$_2$ nanoparticles. The crystal size, D, of the Eu shells was estimated using the Scherrer equation, $D = 0.9\lambda \, / \, \beta\cos\theta$ [28], where λ is the X-ray wavelength and β is the full width in radians at half-maximum (FWHM) of the diffraction peak at the Bragg angle of θ. The Eu nanocrystal shell on the SiO$_2$ nanoparticles was determined to be 1.3 nm in size, which is consistent with the SEM image. The nanostructure of the SiO$_2$/Eu particles was evidently not affected by the coordination with phen, as determined from XRPD analysis and SEM images (Figs. S3 and S4).

Fig. 4 presents the luminescence spectra of SiO$_2$/Eu/phen nanoparticles. Under UV light, the nanoparticles generated a bright red emission originating from the ff transitions of Eu^{III}. Since the SiO$_2$/Eu without phen cannot emit in any wavelength regions, this red emission may occur through energy transfer from the phen to the Eu^{III} at the interface of the SiO$_2$/Eu nanoparticles. Interestingly, the emission colour of the SiO$_2$/Eu/phen nanoparticles could be tuned from red to blue by sintering at 200 °C; after sintering for 60 min, the emission colour was completely changed to blue. The as-prepared SiO$_2$/Eu/phen exhibited sharp emission bands at 578.2, 589.5, 611.1, 651.1 and 700.5 nm, assigned to the $^5D_0 \rightarrow {}^7F_0$, $^5D_0 \rightarrow {}^7F_1$, $^5D_0 \rightarrow {}^7F_2$, $^5D_0 \rightarrow {}^7F_3$ and $^5D_0 \rightarrow {}^7F_4$ transitions of Eu^{III}, respectively. Excitation spectra monitored at the ff emission band position correspond to the $\pi\pi^\star$ transition of phen (Fig. S5), confirming that energy transfer from the phen to the Eu^{III} was occurring within the nanoparticles. The red emission band was decreased following sintering at 200 °C and replaced by a broad blue emission band at approximately 434 nm (Fig. S6). This broad emission was the result of the allowed electric dipole $4f^65d \rightarrow 4f^7$ transition of Eu^{II}, via an allowed transition of Eu^{II} rather than energy transfer from the phen. The Eu3d XPS bands in Fig. 5 provided evidence for the reduction of Eu^{III} to Eu^{II} at the interface between the SiO$_2$ and the phen. Eu3d XPS bands corresponding to Eu^{III} were observed at 1135.4 and 1165.2 eV in the case of the as-prepared SiO$_2$/Eu/phen nanoparticles, while the sintered nanoparticles generated corresponding bands at lower energies (1126.2 and 1155.8 eV), assigned to Eu^{II} [29,30].

It is noteworthy that the interfacial SiO$_2$/Eu/phen structure allowed the blue emissive Eu^{II} to be prepared in air and at the relatively low temperature of 200 °C. The morphology and thermal stability of the nanoparticles did not change before and after the sintering process, as shown in TGA and SEM images (Figs. S7 and S8). This transition to Eu^{II} was also stable; the blue emission properties of the material were maintained for more than three months. This reduction phenomenon of Eu was not observed in SiO$_2$/Eu nanoparticles without phen and a pure Eu complex with phen. The reduction of Eu^{III} to Eu^{II} in a specially prepared matrix with a rigid inorganic crystal structure following high temperature treatment in air has been reported, and has been explained by a charge compensation model [31–33]. In the present reduction system, Eu ions were present at the interfaces between SiO$_2$ nanoparticles and phen ligands, and the SiO$_2$ surface acted as a rigid host while the phen functioned as an electron donor through coordination bonds. Thus, the reduced Eu^{II} state can be formed and protected from reaction with oxygen by the surrounding SiO$_2$ and phen. To the best of our knowledge, this is the first reported fabrication of a stable Eu^{II}-based emissive material using mild conditions (reaction in air and at low temperature) and an organic-inorganic hybrid nanostructure.

To quantitatively assess the effect of phen on the reduction of Eu ions at the interface, the absolute luminescence quantum yields, ϕ_{ff}, and lifetimes, τ_{ff}, of the SiO$_2$/Eu/phen nanoparticles were estimated. The as-prepared SiO$_2$/Eu/phen generated a Eu^{III} ff emission with $\phi_{ff} = 5.3\%$ and $\tau_{ff} = 486.3\,\mu$s (Fig. S9). The total emission quantum yield of Eu^{III} sensitized by the ligand phen (ϕ_{ff}) was determined by the triplet yield of the ligand (ϕ_{ISC}), the efficiency of energy transfer (η_{EnT}) and the efficiency of the metal centred luminescence (η_{Ln}), as follows [34]:
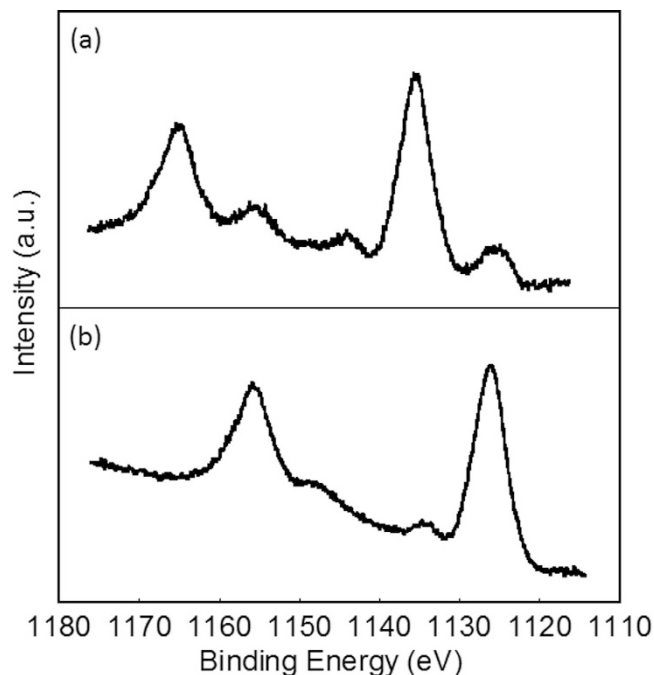
Figure 5. Eu3d XPS bands of a) as-prepared and **b)** sintered SiO_2/Eu/phen nanoparticles.

$$\phi_{ff} = \phi_{ISC} \times \eta_{EnT} \times \eta_{Ln} \tag{1}$$

Because of the $n\pi^\star$ character of the ligand and the high spin-orbit coupling constants of the lanthanide ion, it can be assumed that ϕ_{ISC} was approximately 1 [35,36]. The value of η_{Ln} can be calculated from the observed emission lifetime (τ_{ff}) and the radiative rate constant (k_R) of the lanthanide ion, as shown below.

$$\eta_{Ln} = k_R \times \tau_{ff} \tag{2}$$

The k_R value of the emissive excited state, $^5D_0$, is the sum of the spontaneous emission probabilities, $A(0, J)$, to the lower ^7F_J levels in Eu^{III}, and can in turn be calculated from the following equation.

$$k_R = \sum_J A(0, J) = A(0, 1) \times \frac{I_{Total}}{I(0, 1)} \tag{3}$$

Here, $I_{Total}/I(0, 1)$ is the ratio of the total integrated intensity of the corrected Eu^{III} emission spectrum to the intensity of the $^5D_0 \rightarrow {}^7F_1$ band. In this case, we obtained a value of 6.21 for $I_{Total}/I(0, 1)$. The spontaneous emission probability of the magnetic dipole $^5D_0 \rightarrow {}^7F_1$ transition, $A(0, 1)$, is virtually independent of the ligand field or the environment of the ions, and can be determined directly from the theoretically calculated dipole strength as follows.

$$A(J, J') = \frac{64\pi^4 \sigma^3 n^3}{3h(2J + 1)} \times S_{MDT}(J, J') \tag{4}$$

Here, σ is the energy gap between the excited ($^5D_0$) and the final ($^7F_1$) states ($\sigma = 16963\,\text{cm}^{-1}$), n is the refractive index (1.5 for the solid state metal-organic complex)[37] and $S_{MDT}(J, J')$ is the magnetic dipole strength[38]. The latter parameter has been calculated theoretically for the $^5D_0 \rightarrow {}^7F_1$ transition of Eu^{III} and found to have a value of 884×10^{-8} Debye^2,[39] leading to $45.7\,\text{s}^{-1}$ for $A(0, 1)$.

The calculated values for k_R and η_{Ln} (from Equations 2 and 3) obtained using the experimentally determined values of τ_{ff} and $I_{Total}/I(0, 1)$ were $283.2\,\text{s}^{-1}$ and 0.384, respectively. The k_R value was less than that of a pure complex with phen (*ex.* $569.6\,\text{s}^{-1}$ in [Eu(phen)$_2$(NO$_3$)$_3$], Fig. S10 and Table S1), indicating that a more highly symmetrical environment was present in the vicinity of the Eu^{III} ions in the SiO_2/Eu nanoparticles. These highly symmetrical conditions allow the Eu ion to function as a stable inorganic emissive compound. Thus, this organic-inorganic hybrid material simultaneously exhibits the photochemical and structural properties of both organic and inorganic materials, which may be responsible for the unusual reduction of Eu^{III} to Eu^{II} in air at a low temperature. From Equation 1, the value of the energy transfer efficiency, η_{EnT}, from phen to Eu^{III} on the SiO_2/Eu nanoparticles is estimated to be 0.385. In contrast, the value of η_{EnT} is almost 1 in the solid state molecular structure [Eu(phen)$_2$(NO$_3$)$_3$]. The
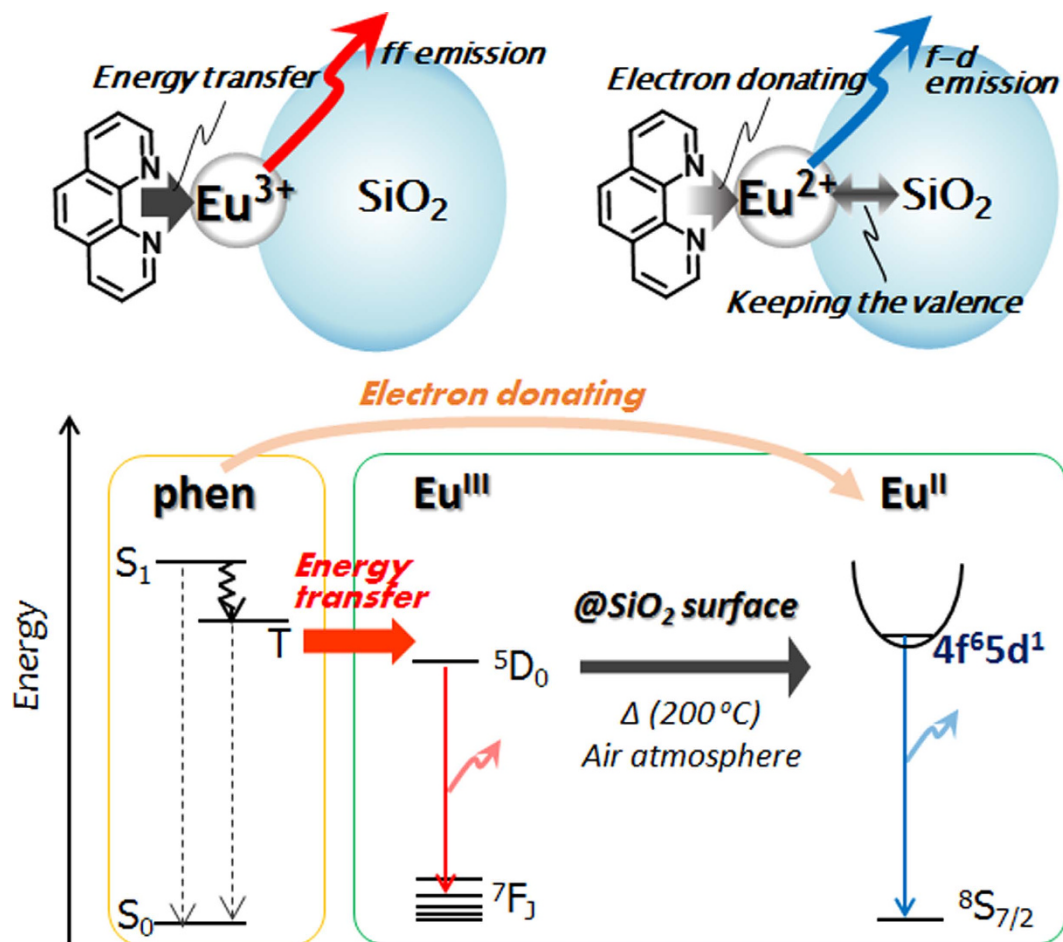
Figure 6. Energy diagram for as-prepared and sintered SiO$_2$/Eu/phen nanoparticles.

considerably lower η_{EnT} of the SiO$_2$/Eu/phen nanostructure suggests the existence of an alternative energy migration pathway, such as a ligand (phen) to metal (Eu^{III}) charge transfer (LMCT)[40–43]. The presence of an LMCT pathway indicates the ability of the phen to donate electrons to Eu ions, which may result in the unusual reduction of Eu^{III} to Eu^{II} through a thermally activated process. In this reduction-induced emission system, SiO$_2$ nanoparticles as host materials is supposed to keep the valence of Eu^{II} at the interface.

After sintering at 200 °C, a blue emission band due to the Eu^{II} appeared around 435 nm with $\tau = 11.59\,\mu s$ (Fig. S9). The ϕ of the Eu^{II} in the SiO$_2$/Eu/phen eventually reached a value of 7.2%, higher than that of the Eu^{III} state because of the allowed electric dipole 4f^{6}5d $\rightarrow$ 4f^7 transition. Following sintering at 200 °C, Eu^{III} emission was no longer observed. The surfaces of the SiO$_2$/Eu particles were less likely to be attacked by oxygen because of the coordination with phen, and therefore the Eu^{II} state in the SiO$_2$/Eu/phen was very stable and the ions were prevented from being re-oxidized, even in air. The reduction-induced emission phenomena are summarized by the energy diagram in Fig. 6.

Conclusions

In conclusion, we discovered a novel emission phenomenon associated with the reduction process in an interfacial complex formed on inorganic nanoparticles. In this study, a Eu-coated SiO$_2$ nanostructure was developed, consisting of an interfacial complex of Eu and phen at the solid surfaces. The as-prepared SiO$_2$/Eu/phen nanoparticles exhibited sharp red emission via energy transfer from the phen to the Eu^{III}. After sintering at 200 °C in air, the emission was tuned from red to blue. The blue emission resulted from Eu^{II}, indicating that the unusual reduction of Eu^{III} to Eu^{II} under mild conditions was successfully accomplished for the first time. The existence of two different stable oxidation states with characteristic emissions, blue emissive Eu^{II} and red emissive Eu^{III}, suggests significant potential applications as novel luminescent materials with inorganic-organic hybrid structures. For instance, our colour-tunable SiO$_2$ nanoparticles with Eu ions, as having less toxicity, will be greatly beneficial for biological and biomedical applications. Additionally, this redox-active interface between inorganic and organic materials may provide a new photon energy conversion system such as artificial photosyntheses and solar cells. Studies

are now underway to fabricate a photoelectron conversion system based on the Eu interfacial complex by way of using a metal oxide with an appropriate redox potential, such as mesoscopic TiO_2.

Methods

Sample preparation. SiO_2/Eu nanoparticles were prepared by the sol-gel method. SiO_2 nanoparticles (QS-20, Tokuyama Co.) were suspended in ethanol (10 wt%) followed by the addition of a 50 mM ethanol solution of $EuCl_3$ (Kanto Chemicals Co., Inc.) at 70 °C for 30 min. The resulting colloidal suspension containing SiO_2 and Eu ions was dropped onto a quartz substrate that had been sequentially cleaned ultrasonically in acetone, isopropanol and ultra-pure water (10 min in each solvent). Following treatment at 110 °C for 15 min, SiO_2 nanoparticles coated with Eu^{III} oxides or hydroxides were obtained. To generate complexation at the particle surfaces, the glass substrate holding the nanoparticles was immersed in a 1 mM ethanol solution of phen (Kanto Chemicals Co., Inc.) at 75 °C for 60 min. After drying, the nanoparticles were further sintered at 200 °C in air.

Apparatus. SEM images were obtained on a ZEISS ULTRA 55 microscope equipped with a secondary in-lens electron detector, together with a Bruker-QUANTAX detector for EDS studies. X-ray photoelectron spectroscopy (XPS) was performed using a KRATOS AXIS ULTRA DLD equipped with a monochromatic Al-Kα X-ray source (1253.6 eV); the binding energies were calibrated at the Au 4f level (84.0 eV). Synchrotron X-ray powder diffraction (XRPD) patterns were obtained with a large Debye-Scherrer camera installed at the SPring-8 BL02B2 beamline, using an imaging plate as the detector[44] and an incident X-ray wavelength of 0.99933 Å. Luminescence spectra were recorded on a Horiba Jobin-Ybon Fluorolog 3–22 with a UV cut filter. The emission decay curves were acquired using a Quantaurus-*T*au C11367-12 (Hamamatsu Photonics K. K.) with excitation via a xenon flash lamp with a band-path filter ($\lambda_{ex} = 280$ nm). Fluorescence quantum yields were measured by using a C9920-02 Absolute PL Quantum Yield Measurement System (Hamamatsu Photonics K. K.)[45–47].

References

1. Carlos, L. D., Ferreira, R. A. S., Bermudez, V. Z. & Ribeiro, S. J. L. Lanthanide-Containing Light-Emitting Organic-Inorganic Hybrids: A Bet on the Future. *Adv. Mater.* **21,** 509–534 (2009).
2. Guloy, A. M., Tang, Z., Miranda, P. B. & Srdanov, V. I. A New Luminescent Organic–Inorganic Hybrid Compound with Large Optical Nonlinearity. *Adv. Mater.* **13,** 833–837 (2001).
3. Hao, X.-L. *et al.* A new organic–inorganic hybrid compound based on lanthanide-organic chain and Keggin-type polyoxometalate. *Inorg. Chem. Commun.* **14,** 1698–1702 (2011).
4. Schulze, M. *et al.* Reversible Photoswitching of the Interfacial Nonlinear Optical Response. *J. Phys. Chem. Lett.* **6,** 505–509 (2015).
5. Koutselas, I. *et al.* Some Unconventional Organic−Inorganic Hybrid Low-Dimensional Semiconductors and Related Light-Emitting Devices. *J. Phys. Chem. C* **115,** 8475–8483 (2011).
6. Piersimoni, F. *et al.* Charge Transfer Absorption and Emission at ZnO/Organic Interfaces. *J. Phys. Chem. Lett.* **6,** 500–504 (2015).
7. Lin, Z. Q. & Zhao, L. Crafting semiconductor organic-inorganic nanocomposites via placing conjugated polymers in intimate contact with nanocrystals for hybrid solar cells. *Adv. Mater.* **24,** 4353–4368 (2012).
8. Akhtar, N. *et al.* Design of nolecuyle-based magnetic conductor. *Nano Research* **7,** 1832–1842 (2014).
9. Zhang,Y. *et al.* Fe_3O_4/PVIM-Ni^{2+} Magnetic Composite Microspheres for Highly Specific Separation of Histidine-Rich Proteins. *ACS Appl. Mater. Interfaces* **6,** 8836–8844 (2014).
10. Fei, J. & Li, J. Controlled Preparation of Porous TiO_2 –Ag Nanostructures through Supramolecular Assembly for Plasmon-Enhanced Photocatalysis. *Adv. Mater.* **27,** 314–319 (2015).
11. Youn, D. *et al.* Highly Active and Stable Hydrogen Evolution Electrocatalysts Based on Molybdenum Compounds on Carbon Nanotube–Graphene Hybrid Support. *ACS Nano* **8,** 5164–5173 (2014).
12. Dorenbos, P. Energy of the first $4f^7$-$4f^65d$ transition of Eu^{2+} in inorganic compounds. *J. Lumin.* **104,** 239–260 (2003).
13. Matsuzawa, T., Aoki, Y., Takeuchi, N. & Murayama, Y. A New Long Phosphorescent Phosphor with High Brightness, $SrAl_2O_4$:Eu^{2+},Dy^{3+}. *J. Electrochem. Soc.* **143,** 2670–2673 (1996).
14. Suriyamurthy, N. & Panigrahi, B. S. Effects of non-stoichiometry and substitution on photoluminescence and afterglow luminescence of $Sr_4Al_{14}O_{25}$:Eu^{2+}, Dy^{3+} phosphor. *J. Lumin.* **128,** 1809–1814 (2008).
15. Qiao, X. *et al.* Synthesis and Luminescence Properties of Blue-Emitting Phosphor Eu^{2+}-Doped Zinc Fluoro-Phosphate $Zn_2[PO_4]$F. *J. Am. Ceram. Soc.* **97,** 3561–3567 (2014).
16. Dutczak, D., Ronda, C., Jüstel, T. & Meijerink, A. Anomalous trapped exciton and d-f emission in $Sr_4Al_{14}O_{25}$:Eu^{2+}. *J. Phys. Chem. A* **118,** 1617–1621 (2014).
17. Li, K. *et al.* Color-Tunable Luminescence and Energy Transfer Properties of $Ca_9Mg(PO_4)_6F_2$:Eu^{2+}, Mn^{2+} Phosphors for UV-LEDs. *J. Chem. Phys. C* **118,** 11026–11034 (2014).
18. Liu, B., Wang, Y., Zhou, J., Zhang, F. & Wang, Z. The reduction of Eu^{3+} to Eu^{2+} in $BaMgAl_{10}O_{17}$: Eu and the photoluminescence properties of $BaMgAl_{10}O_{17}$: Eu^{2+} phosphor. *J. Appl. Phys.* **106,** 053102–5 (2009).
19. Xie, H. *et al.* Abnormal reduction, $Eu^{3+} \rightarrow Eu^{2+}$, and defect centers in Eu^{3+}-doped pollucite, $CsAlSi_2O_6$, prepared in an oxidizing atmosphere. *Inorg. Chem.* **53,** 827–834 (2014).
20. Lian, Z., Wang, J., Lv, Y., Wang, S. & Su, Q. The reduction of Eu^{3+} to Eu^{2+} in air and luminescence properties of Eu^{2+} activated ZnO–B_2O_3–P_2O_5 glasses. *J. Alloys Compd.* **430,** 257–261 (2007).
21. Peng, M. & Hong, G. Reduction from Eu^{3+} to Eu^{2+} in $BaAl_2O_4$:Eu phosphor prepared in an oxidizing atmosphere and luminescent properties of $BaAl_2O_4$:Eu. *J. Lumin.* **127,** 735–740 (2007).
22. Ishii, A. & Miyasaka, T. A high voltage organic–inorganic hybrid photovoltaic cell sensitized with metal–ligand interfacial complexes. *Chem. Commun.* **48,** 9900–9902 (2012).
23. Ishii, A. & Miyasaka, T. A Metallocene Molecular Complex as Visible-Light Absorber for High-Voltage Organic–Inorganic Hybrid Photovoltaic Cells. *Chem Phys Chem* **15,** 1028–1032 (2014).
24. Zheng, Y.-Q., Zhou, L.-X., Lin, J.-L. & Zhang, S.-W. Syntheses and crystal structures of Ln(phen)$_2$(NO$_3$)$_3$ with Ln = Pr, Nd, Sm, Eu, Dy, and phen = 1,10-phenanthroline. *Z. Anorg. Allg. Chem.* **627,** 1643–1646 (2001).
25. Wan, Y., Zhang, L., Jin, L., Gao, S. & Lu, S. High-Dimensional Architectures from the Self-Assembly of Lanthanide Ions with Benzenedicarboxylates and 1,10-Phenanthroline. *Inorg. Chem.* **42,** 4985–4994 (2003).

26. Ishii, A. *et al.* Novel emission properties of melem caused by the heavy metal effect of lanthanides(III) in a LB film. *Photochem. Photobiol. Sci.* **6,** 804–809 (2007).
27. Wang, Y. D., Ma, C. L., Li, H. D. & Zhang, S. Synthesis and characterization of the composite of SnO_2 nanoparticles coated on SiO_2 microspheres. *Mater. Chem. Phys.* **107,** 248–253 (2008).
28. Scherrer, P. Determination of the size and internal structure of colloidal particles using X-rays. *Nachr. Goettinger Gesell.* **2,** 98–100 (1918).
29. Schneider, W.-D., Laubschat, C., Nowik, I. & Kaindl, G. Shake-up excitations and core-hole screening in Eu systems. *Phys. Rev. B* **24,** 5422–5425 (1981).
30. Han, M., Oh, S.-J., Park, J. H. & Park, H. L. X-ray photoelectron spectroscopy study of CaS:Eu and SrS:Eu phosphors. *J. Appl. Phys.* **73,** 4546–4549 (1993).
31. Dwivedi, Y. & Rai, S. B. Blue and red emission from Eu doped barium tetraborate crystals. *J. Am. Ceram. Soc.* **93,** 727–731 (2010).
32. Peng, M., Pei, Z., Hong, G. & Su, Q. The reducing of Eu^{3+} to Eu^{2+} in $BaMgSiO_4$:Eu prepared in air and the luminescence of $BaMgSiO_4$:Eu^{2+} phosphor. *J. Mater. Chem.* **13,** 1202–1205 (2003).
33. Pei, Z., Zeng, Q. & Su, Q. The application and a substitution defect model for $Eu^{3+} \rightarrow Eu^{2+}$ reduction in non-reducing atmospheres in borates containing BO_4 anion groups. *J. Phys. Chem. Solids* **61,** 9–12 (2000).
34. Beeby, A., Bushby, L. M., Maffeo, D. & Williams, J. A. G. Intramolecular sensitization of lanthanide(III) luminescence by acetophenone-containing ligands: the critical effect of para-substituents and solvent. *J. Chem. Soc. Dalton Trans.* **1,** 48–54 (2002).
35. El-Sayed, M. A. Spin-Orbit Coupling and the Radiationless Processes in Nitrogen Heterocyclics. *J. Chem. Phys.* **38,** 2834–2838 (1963).
36. Bhaumik, M. L. & El-Sayed, M. A. Mechanism and Rate of the Intramolecular Energy Transfer Process in RareEarth Chelates. *J. Chem. Phys.* **42,** 787–788 (1965).
37. Pavithran, R. *et al.* 3-Phenyl-4-benzoyl-5-isoxazolonate Complex of Eu^{3+} with Tri-*n*-octylphosphine Oxide as a Promising Light-Conversion Molecular Device. *Inorg. Chem.* **45,** 2184–2192 (2006).
38. Weber, M. J., Varitimos, T. E. & Matsinger, B. H. Optical Intensities of Rare-Earth Ions in Yttrium Orthoaluminate. *Phys. Rev. B* **8,** 47–53 (1973).
39. Kirby, A. F. & Richardson, F. S. Detailed analysis of the optical absorption and emission spectra of Eu^{3+} in the trigonal (C_3) $Eu(DBM)_3$.H_2O system. *J. Phys. Chem.* **87,** 2544–2556 (1983).
40. Puntus, L. N., Lyssenko, K. A., Pekareva, I. S. & Bünzli, J.-C. G. Intermolecular Interactions as Actors in Energy-Transfer Processes in Lanthanide Complexes with 2,2'-Bipyridine. *J. Phys. Chem. B* **113,** 9265–9277 (2009).
41. Matthes, P. R. *et al.* The Series of Rare Earth Complexes [$Ln_2Cl_6(\mu$-4,4'-bipy)(py)$_6$], Ln=Y, Pr, Nd, Sm-Yb: A Molecular Model System for Luminescence Properties in MOFs Based on $LnCl_3$ and 4,4'-Bipyridine. *Chem. Eur. J.* **19,** 17369–17378 (2013).
42. Bassett, A. P. *et al.* Highly Luminescent, Triple- and Quadruple-Stranded, Dinuclear Eu, Nd, and Sm(III) Lanthanide Complexes Based on Bis-Diketonate Ligands. *J. Am. Chem. Soc.* **126,** 9413–9424 (2004).
43. Räsänen, M. *et al.* Study on photophysical properties of Eu(III) complexes with aromatic β-diketones – Role of charge transfer states in the energy migration. *J. Lumin.* **146,** 211–217 (2014).
44. Ohashi, H. *et al.* Low-glancing-angle x-ray diffraction study on the relationship between crystallinity and properties of C 60 field effect transistor. *Appl. Phys. Lett.* **84,** 520–522 (2004).
45. Kawamura, Y., Sasabe, H. & Adachi, C. Quantum yields were determined by the absolute method using an integrating sphere. *Jpn. J. Appl. Phys.* **43,** 7729–7730 (2004).
46. Suzuki, K. *et al.* Reevaluation of absolute luminescence quantum yields of standard solutions using a spectrometer with an integrating sphere and a back-thinned CCD detector. *Phys. Chem. Chem. Phys.* **11,** 9850–9860 (2009).
47. Kobayashi, A., Suzuki, K., Yoshihara, T. & Tobita, S. Absolute Measurements of Photoluminescence Quantum Yields of 1-Halonaphthalenes in 77K Rigid Solution Using an Integrating Sphere Instrument. *Chem. Lett.* **39,** 282–283 (2010).

Acknowledgements

Author Contributions

A.I. designed this study, performed experiments, and wrote the manuscript. M.H. discussed the results and contributed to the final version of the paper.

Additional Information

Supplementary information accompanies this paper at http://www.nature.com/srep

Competing financial interests: The authors declare no competing financial interests.

How to cite this article: Ishii, A. and Hasegawa, M. An Interfacial Europium Complex on SiO2 Nanoparticles: Reduction-Induced Blue Emission System. *Sci. Rep.* **5**, 11714; doi: 10.1038/srep11714 (2015).